Nanoscale

Accepted Manuscript

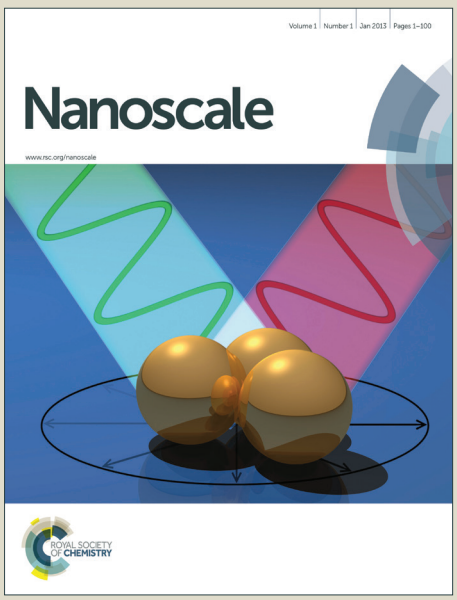

ROYAL SOCIETY OF CHEMISTRY

www.rsc.org/nanoscale

Probing nanoscale graphene-liquid interfacial interactions via Ultrasonic Force Spectroscopy

Benjamin J. Robinson and Oleg V. Kolosov*

Physics Department, Lancaster University, Lancaster, LA1 4YB, UK

o.kolosov@lancaster.ac.uk, http://www.nano-science.com

Abstract

We probe the interfacial forces in graphene-air and graphene-liquid environments with nanoscale resolution. Experimentally, probe 'snap-in' to contact, in scanning probe microscopy, is overcome by combining the ultrasonic force spectroscopy (UFS) approach and MHz frequency range harmonic oscillation of the sample thereby sweeping the tip-surface dynamically from separated to indented state across the region of intimate interface contact. We measured the force interaction between nanoscale probe tip and graphene, graphite and reference SiO_2 surface in ambient, polar and non-polar liquid environments. Via modelling we estimated the decay length of the force interaction in water to be 0.25 – 0.75 nm, equivalent to 1-3 monolayers, and interfacial effective stiffness at these distances associated with the liquid layer was an order of magnitude greater for non-polar than for polar liquid environment. During the elastic indentation at increased forces, the effective Young modulus of graphene was shown only to be slightly reduced in ambient environment while experiencing significant reduction by a factor of 3 in non-polar dodecane environment.

I. Introduction.

If the potential of graphene,[1] and the related family of newly isolated ultrathin materials, such as MoS_2[2] and GaSe,[3] for the next generation of nanoelectromechanical systems,[4, 5] energy storage[6-8] and optical [9, 10] devices is to be realised, there is a need to understand the interaction of these two-dimensional (2D) layers with the substrate and local environment. A key part of this is interfacial nano-mechanics of normal forces[11-15] and friction[16-18] studied in both ambient as well as liquid environments.[19] Here, we present a methodology, ultrasonic force spectroscopy (UFS), to probe force interactions in the interfacial layers of graphene-air and graphene-liquid environments with nanoscale resolution.

To achieve this, it is essential to access, in a controlled manner, the narrow distance range corresponding to the establishment and breaking of a nanoscale probe–sample contact. Unfortunately, this distance range is not readily accessible for well-established atomic force microscopy (AFM) techniques due to sudden probe 'snap-in' to contact, which occurs as soon as the gradient of the attractive forces becomes larger than the spring constant of the cantilever supporting the probe tip. The snap-in can be avoided by a significant increase of the spring constant above the force gradient, however this will inevitably drastically reduce SPM sensitivity to the probed forces.[20]

In this paper we show that this trade-off can be overcome by exploiting the nonlinear response of the tip-sample interaction during the approach-retract behaviour of a contact mode AFM probe in ambient and liquid environments using the UFS approach stemming from the ultrasonic force microscopy (UFM) principle of non-linear detection of contact forces.[21] In UFS the sample is oscillated at high frequency of several MHz[22] well above inherent probe or system resonances. At these frequencies the tip-cantilever system becomes dynamically frozen resulting in controlled periodic sinusoidal modulation of the tip-surface distance passing from a non-contact state through to full indentation.[23] Then the nonlinear nature of the force-vs-indentation dependence results in the change of the average net force acting on the tip, which is then easily measured as a DC displacement of a compliant at low frequency, and therefore highly force sensitive, cantilever.

It has been shown elsewhere using UFM that liquids form solid-like cushions on graphene surfaces, through the application of ultrasonic excitation of the sample, significantly modifying the local tribological properties.[24, 25] Whereas the previous study concerned the modification of surface lateral forces we now investigate the modification of the normal forces at the graphene–environment interface. The UFM operation in liquid environments[26] remains relatively unexplored and questions remain about the disruptive influence of the radiation pressure, induced by the ultrasonic wave propagation through the liquid medium, on the cantilever during UFM scanning. Furthermore the exact effects arising from the combined dynamic stiffness of the liquid layer and sample averaged over the contact/non-contact period of oscillation require further exploration. Using exfoliated few layer graphene (FLG), graphite and SiO_2 we have studied a comprehensive set of systems composed of combination of hydrophobic or hydrophilic surfaces immersed in both polar and non-polar liquids. We have compared the experimental data with a series of models based upon Hertzian sample-probe interactions both with and without a liquid layer[27] allowing the estimation of the

interfacial effective stiffness and decay length of interfacial forces, in both polar and non-polar environments.

II. Probe – sample interaction models

In UFS measurements the sample is oscillated at ultrasonic (high frequency, HF) frequency f and at amplitude a, by an external piezoceramic transducer, modulated with a low frequency (LF) signal to aid detection. Due to extreme dynamical rigidity of the cantilever [21] at HF > 2-4 MHz the vibration of the sample is not transferred to the cantilever and therefore one can safely assume that the tip-surface distance is also oscillated at the same HF f and amplitude a[28]. Due to the highly nonlinear dependence of the interaction force on the tip-surface distance[29, 30] such oscillation is "rectified" producing an additional "ultrasonic" force at the modulation frequency and hence an additional displacement of the cantilever z_a. z_a has been shown to be directly dependent on a, effective sample elastic modulus E^*, normal force F_N and cantilever stiffness k_c. In this study, this nonlinear response z_a is directly measured *via* lock-in amplifier as a function of F_N and a and compared to modelling of the probe-sample interaction. A more detailed description of UFM operation and the origin of the nonlinear response are given in supporting notes 1 and 2 and specific experimental details in the methods section below. Comparison of FLG images obtained by contact and tapping AFM and UFM are shown in supplementary note 6.

In order to understand the behaviour of the normal force as a function of probe-sample indentation, here, we employ a three component contact mechanics model describing the classical Hertzian contact force between a sphere and flat plane (F_{Hertz})[31], van der Waals adhesive[32] between tip and sample (F_{DMT}) (the Derjaguin-Muller-Toporov model) and short-range hydration forces in water, (F_{Hyd}).[27] A supported layer model is not required here as the maximum indentation probed is 0.5-0.65 nm into a sample of 2.1 nm thickness.[33] The precise role of F_{Hyd} is still not fully understood, however there is extensive experimental evidence of its importance on separation length scales of 0 to 10 nm[34] where it provides a good quantitative description of hydrophobic forces which in some systems can be stronger than the van der Waals attractions.[35] F_{Hyd} is repulsive for hydrophilic and attractive for hydrophobic surfaces. The total force between tip and sample (F_{ts}) can be presented as a function of indentation (h)

$$F_{ts}(h) = F_{Hertz}(h) + F_{DMT}(h) + F_{hyd}(h)$$

The individual components are given in table I, where out of contact is denoted as $h > 0$ and in contact as $h < 0$, where E^* is the reduced elastic modulus such that

$$\frac{1}{E^*} = \frac{(1-\upsilon_{tip}^2)}{E_{tip}} + \frac{(1-\upsilon_{sample}^2)}{E_{sample}}$$

$\upsilon_{tip,sample}$ and $E_{tip/sample}$ are the Poisson's ratio and Young's modulus for the tip and sample, respectively, R_t is the radius of the tip, γ is the surface energy of the sample, p_l is an empirically determined scaling factor where the sign of p_l determines whether the interaction is hydrophilic or hydrophobic and λ is hydration decay length.

Table 1. Contact and non-contact equations describing the Hertz, DMT and hydration force models.

	$F_{Hertz}(h)$	$F_{DMT}(h)$	$F_{hyd}(h)$
$h > 0$	0	0	$2\pi R_t^2 p_l \exp\left(-\frac{h}{\lambda}\right)$
$h < 0$	$\frac{4}{3}E^*\sqrt{R_t}h^{3/2}$	$-2\pi R_t \gamma$	$2\pi R_t^2 p_h$

The force-vs-indentation dependence for typical values of force components, F_{Hertz}, $F_{Hertz} + F_{DMT}$ and $F_{Hertz} + F_{DMT} + F_{hyd}$ are shown in Fig 1. for graphene sample and Si AFM tip in ambient and water environment. Here we can see that due to the significant non-contact portion of the UFM oscillation the average forces sensed by the probe are modified (as shown in Fig S2), namely, if a liquid layer is present on the surface of the sample the response will be a 'composite' response comprising of the contact stiffness of the sample and forces produced in the liquid layer.

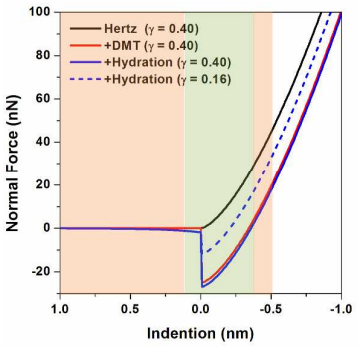

FIG 1. Examples of typical force-vs-indentation dependence for the Hertz, DMT and Hydration models of

adhesion for graphene in ambient and water environments. Green shaded region corresponds to the range of tip-surface distances probed by UFS at low ultrasonic amplitudes a_u and orange to high.

To accurately reflect the experimental data the surface energy term (γ) is treated as a variable parameter, such that the maximal adhesive force of the model matches the experimentally measured value. In Fig 1 the solid blue line represents the simulated water immersion case with $\gamma = 0.40$ Jm^{-2}, equivalent to adhesion in ambient environment, whilst the dashed blue line is the same model but with $\gamma = 0.16$ Jm^{-2}, which corresponding to the experimentally observed adhesion in water immersion. These values are similar to reported in the literature[36-38] and reflect the changes we observed in the maximum attractive force. Here, we note a significant change in the magnitude of the force-indentation relation with changing γ; these effects are explored in detail below. Parameters used in the simulations for the materials and environments presented in this paper, are given in Table 2. Values for hydration scaling force and decay were empirically determined and found to be consistent, for water, with literature.[27]

Table 2. Modelling parameters.	
Radius of tip (nm)	$R_t = 10$
Cantilever stiffness (Nm^{-1})	$k_c = 0.2$
Young's modulus (GPa)	$E_{graphite} = 10$ $E_{SiO2} = 55$ $E_{graphene\perp} = 35$ $E_{tip} = 166$
Poisson's ratio	$\upsilon_{graphite} = 0.25$ $\upsilon_{SiO2} = 0.27$ $\upsilon_{graphene} = 0.17$ $\upsilon_{tip} = 0.22$
Hydration decay length (nm)	$\lambda_{H2O} = 0.25$ $\lambda_{C12H26} = 0.39$
Hydration force scaling	$p_{l(H2O)} = 3 \times 10^6$ $p_{l(C12H26)} = 3 \times 10^7$
Effective surface energy in ambient, water and dodecane (Jm^{-2})	$\gamma_{graphene\text{-}amb} = 0.40$ $\gamma_{graphite\text{-}amb} = 0.27$ $\gamma_{SiO2\text{-}amb} = 0.34$ $\gamma_{graphene\text{-}H2O} = 0.16$ $\gamma_{SiO2\text{-}H2O} = 0.11$

	$\gamma_{graphene\text{-}C12H26} = 0.03$ $\gamma_{SiO2\text{-}C12H26} = 0.07$
Graphite and SiO_2 properties are manufacturers stated values, whilst out-of-plane $E_{graphene\perp}$[39] and $\upsilon_{graphene}$,[40] monolithic silicon AFM tip E_{tip} and υ_{tip}[41] are taken from literature. R_t and k_c were experimentally determined by SEM and Sader[42, 43] analysis respectively (see Methods section below). Effective surface energy terms are empirically derived according to the equations in table 1.	

Results and Discussion

UFM nonlinear response in ambient environment

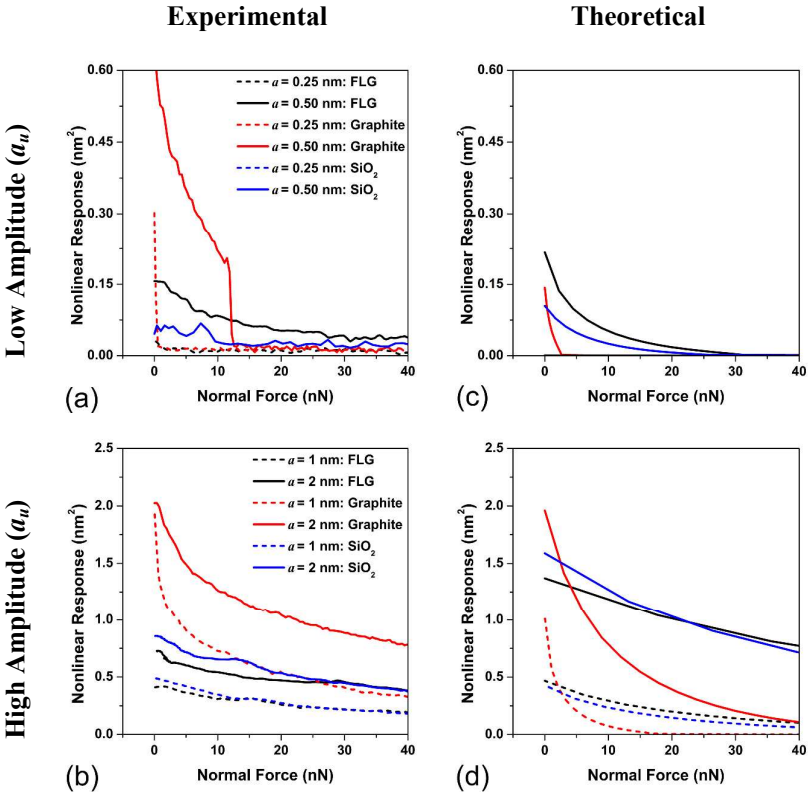

FIG 2. a, b) Experimental UFS response vs normal force (retraction curve) in ambient environment for graphite (red) FLG (black) and SiO_2 (blue) and c, d) corresponding theoretical normal force vs nonlinear responses. For clarity we have shown low amplitude a_u = 0.25nm and 0.5nm and high a_u = 2nm and a_u = 1nm on separate plots where, for each plot, the higher amplitude is the solid line and the lower amplitude the dashed line.

Experimental UFS and simultaneously acquired normal force data were collected for FLG, graphite and SiO_2 in ambient, polar and non-polar environments using measurement procedure described in Methods. The experimentally measured UFS responses for materials in ambient environment are plotted in Fig 2 for low a (0.25 and 0.5 nm) and high a (1 and 2 nm) ultrasonic amplitudes. Here we plot the retraction portion of the curves, that covers a wide range of interaction forces, against matching theoretical simulation that uses DMT approximation (in absence of liquid layer) such that $F_{ts}(d) = F_{Hertz}(d) + F_{DMT}(d)$ using the literature reported simulation parameters from table 2 for each material – FLG, graphite and SiO_2. Curves have been aligned such that a normal force of 0 nN corresponds to the pull-off point of the cantilever hence the breaking of probe-sample solid-solid contact (unprocessed data which has not been normalised to the small probe-sample contact area is shown in Supplementary Note 4).

We note excellent qualitative correlation between the model and experimental data at $a \geq$ 0.5 nm (Fig. 2b vs Fig. 2d). Furthermore, in good agreement with experiment, the model predicts negligible response from all materials at the lowest investigated amplitude, a = 0.25 nm (Fig. 2a and Fig. 2c) corresponding to the threshold amplitude for the observation of nonlinear response. Below this value the ultrasonic amplitude, a, is smaller than the initial indentation h_1, so distance oscillations occur in the almost linear region of the force-vs-distance curve so no "rectification" occurs and ultrasonic force is negligible [21].

We note certain discrepancy between the relative magnitudes of the measured and calculated responses of FLG and SiO_2 relative to graphite, most likely arising in the experimental data due to mass loading effects[44] on the piezotransducer which drives the UFS resulting in dampening of the ultrasonic displacement[45]. At the same time FLG exfoliated directly onto the SiO_2 wafer secures identical amplitude of ultrasonic vibrations and therefore allows direct comparison of the ratios of UFS responses – calculated as amplitude ratio between FLG and SiO_2 UFS response averaged over the common range of normalised normal forces – between 0 and 30 nN from the pull-off point, with standard deviations obtained by repeated measurements in the different points on the sample. Table 3 indicates that these ratios for different amplitudes a are in a reasonable agreement between experimental data and theoretical simulation – the ratios decrease with the increase of the vibration amplitude for both experiment and theory, and they coincide within the error margin. Given that no fitting parameter was used, such correspondence is quite remarkable.

Table 3. Ratios of UFS response for FLG and SiO_2 at various a (ambient environment).

a	Experiment	Theory
0.5 nm	2.16 ± 0.55	1.53 ± 0.23
1 nm	0.95 ± 0.06	1.16 ± 0.11
2 nm	0.90 ± 0.08	0.98 ± 0.07

UFM nonlinear response in liquid environments

Using the same approach, we then probed the same interfaces in polar liquid (DI water) and non-polar liquid (dodecane) environments. The theoretical analysis in this case additionally includes a hydration component with a total force represented as $F_{ts}(d) = F_{Hertz}(d) + F_{DMT}(d) + F_{hyd}(d)$. Experimentally, decrease of the maximum adhesion force when moving from air to water environments is explained by the elimination of meniscus which can form at the tip-sample interface in ambient humidity[33] with DMT contact mechanics at the new adhesive force being a reasonable approximation as discussed elsewhere[46]. Further decrease of adhesion is observed when moving from water to dodecane environment due to the minimisation of van der Waals and electrostatic forces.[47] This decrease is reflected in the experimentally determined effective surface energy terms γ derived from the values for the pull-off force, given in table 2.

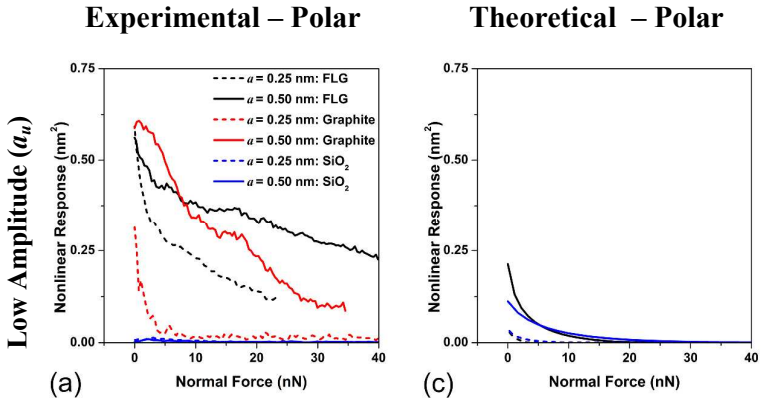

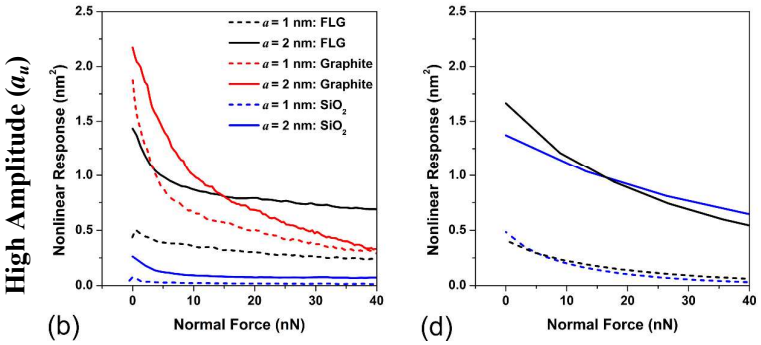

FIG 3. a, b) Experimental UFS vs normal force dependences in polar liquid environment for graphite (red) hydrophobic FLG (black) and hydrophilic SiO_2 (blue) and corresponding c, d) theoretically calculated dependence for hydrophobic FLG (black) and hydrophilic SiO_2 (blue).

Figs. 3 and 4 show separately the experimental and theoretical response of materials in polar water and nonpolar dodecane, respectively, at low (0.25 and 0.5 nm) and high (1 and 2 nm) ultrasonic amplitude a. The free fitting parameter here was the scaling factor,[27] where $p_{l(H20)}$ is 3×10^6 and $p_{l(dodecane)}$ is 3×10^7.

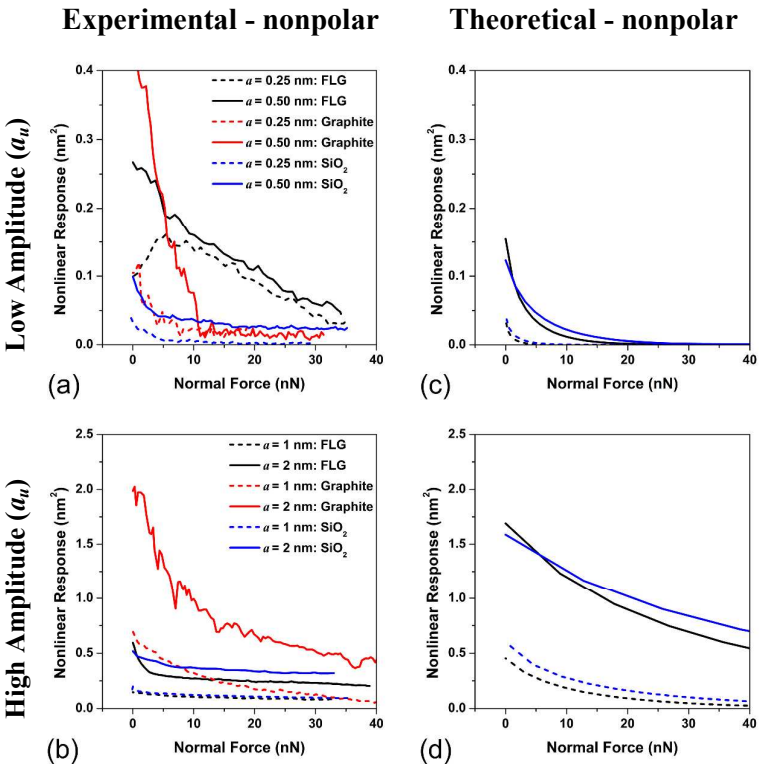

FIG 4. a, b) Experimental UFS vs force in nonpolar liquid environment for graphite (red) FLG (black) and SiO_2 (blue) and corresponding c, d) theoretically calculated response for hydrophobic FLG (black) and hydrophilic SiO_2 (blue).

Figs. 3 and 4 confirm that UFM when the sample-probe system is fully immersed in various liquids[26, 48] can be obtained at a variety of normal forces, with UFS signature clearly different for various materials. Hence, we confirm that the acoustic pressure acting on the entire cantilever area due to the acoustic wave from the immersed piezotransducer that may produce a response similar to the "ultrasonic" force is, in fact, much smaller than the nonlinearly detected "ultrasonic" force originated at the tip apex-surface interface. The response trend was similar to ambient conditions and diminished with the increase of normal force, but with drastically different ratios between UFS response of FLG and SiO_2 in polar vs non-polar liquids. Table 4 shows these ratios for a = 1 and 2 nm (lower amplitudes have low signal-to-noise ratio and were not compared). It is interesting to observe that, in liquid environments for FLG and SiO_2 the UFS response at lower forces was steeply increasing before the pull-off both for low and high amplitudes, differing considerably from in-air experimental data (Fig. 2). Such steep increase indicates that interfacial nonlinearity of force-vs-distance dependence is much more pronounced in underliquid environments – independently of liquid polarity or surface hydrophobicity.

Table 4. Response ratios of FLG and SiO_2 for given a in liquid environments

	Polar		Non-Polar	
a	Experiment	Theory	Experiment	Theory
1 nm	15.86 ± 2.51	0.86 ± 0.10	0.75 ± 0.07	0.74 ± 0.07
2 nm	9.47 ± 1.33	0.99 ± 0.05	0.88 ± 0.19	0.94 ± 0.04

In the qualitative analysis we observe a reasonable correspondence between experiment and theory for UFS response ratios between FLG and SiO_2 in non-polar environment, while the same ratios in polar water environment were order of magnitude higher. This divergence may suggest additional physical effects (discussed in the final section of the paper) and that are not associated with the probed solid-liquid-solid interface discussed in the next section.

Theoretical investigation of sensitivity of UFS nonlinear response to parameters of solid-solid and solid-liquid-solid interfaces.

Ambient environment: Due to the good correlation between experiment and theory in ambient conditions (Fig 2) we investigate two key features - the similarity of the FLG and SiO_2

responses, clearly observed at higher a, and the very different response of graphite. Theoretically we changed intrinsic physical parameters, namely sample elastic moduli E_{sample} and adhesion energy γ. A magnitude of the nonlinear response shown negligible change in the shape, with stable monotonous increase with increase of γ (Fig S3 in Supplementary Informnation), at the same time the dependence on E_{sample} was clearly pronounced (Fig 5).

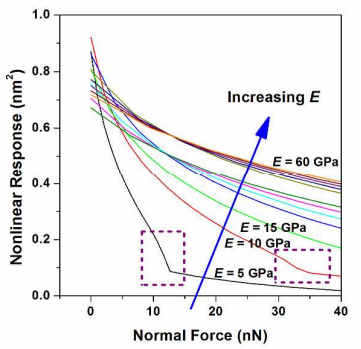

FIG 5. Theoretical analysis of sensitivity of UFS to a material Young Modulus where the arrow shows a region of incrementally increasing value of E_{sample} in the range 5 – 60 GPa in 5 GPa steps (ambient environment).

We interpret the sharp decrease in nonlinear response at low values of sample Young's modulus (Fig. 5, dotted rectangles), that would correspond to graphite systems perpendicular to graphene planes, as the probe indenting into the relatively soft materials that would lead to decrease of ultrasonic force.[49] It is interesting to note that significant nonlinear response for low E materials can only be accessed at low normal forces and higher a. Furthermore, a mainly monotonous relation between γ_{sample} and UFS is generally observed (Supplementary Fig. S3).

Liquid environment: The introduction of the liquid to the system modifies the UFS response due to the dynamic interaction of the nanoscale thin liquid layer in between probe and solid (graphene, graphite and SiO_2) surface. The local nanoscale dynamic properties of such liquid layers are not readily experimentally accessible by other methods[14, 50] and UFS offers a unique opportunity for such studies. The hydration force component applicable to the polar water environment can be described by the hydration decay length, λ, and dimensionless

hydration force scaling factor, p_l, describing effective force interaction of interfacial water layer.[34] The theoretically investigated dependence of UFS response is given in Fig. 6 for λ_{liquid} ranging from 0 to 2 nm in 0.25 nm steps (ca. monolayer thickness of water).

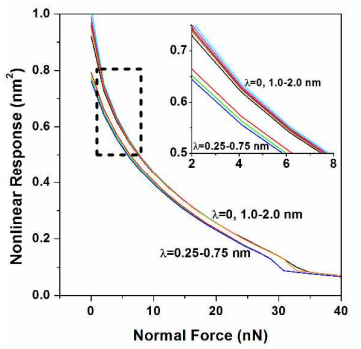

FIG 6. Theoretical analysis of sensitivity of UFS with incrementally increasing value of λ_{liquid} in the range 0 to 2 nm in 0.25 nm steps (E_{sample} = 10 GPa). Insert in b) corresponds to highlighted area of the main plot. Note that λ_{liquid} = 0 is equivalent to the model with no liquid layer.

While for stiff samples (high E_{sample}) a change in decay length produces negligible effect (SI Fig. S4), for softer samples where the influence of the hydration term is expected to be more pronounced, we observe two clear branches (insert in Fig. 6) corresponding to λ_{liquid} = 0 (no liquid layer) and 1.0 – 2.0 nm (thick liquid layer) (upper branch) and intermediate thickness λ_{liquid} = 0.25 – 0.75 nm (lower branch). The return to no liquid layer model-equivalence at $\lambda_{liquid} \geq$ 1nm suggests that, in our model, the hydration force is effective only over the first 1-3 monolayer thicknesses of water; this is good agreement with established literature.[51]

The UFS would be also sensitive to hydration force scaling factor, p_l but with more monotonous dependence. Fig. 7 shows typical high E_{sample} system at a = 1nm for p_l ranging from -3×10^5 to $+3\times10^5$, with similar dependence observable for a low E_{sample} system. However, tip-sample capillary formation is observed even when the sample is strongly hydrophobic graphene;[24] this interaction is dominated by the hydrophilic tip and is therefore always repulsive.

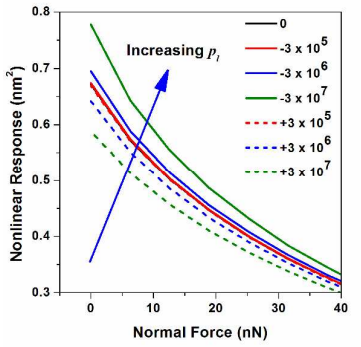

FIG 7. Theoretical analysis of sensitivity of UFS to p_l variation between -3×10^7 to $+3\times10^7$ (in-liquid environment, E_{sample} = 35 GPa).

Monotonous changes in p_l in a similar way to E_{sample} suggest that p_l may be related, in dynamic nanomechanical probing via UFS, to the effective stiffness of the interfacial liquid layer. In a previous study we have shown that liquids, including water, form solid-like cushions when trapped between a AFM probe and ultrasonically excited substrate.[24] We propose therefore, that for these measurements, the hydration term can be associated with affinity of a solvent molecule with the substrate.

Using these parameters we applied the modified liquid layer model to the nonpolar environment where we have assumed the decay length to be ca. one dodecane monolayer thickness (0.39 nm). Direct comparison between the water and dodecane systems was possible due to their similar acoustic impedances and hence resulting amplitude of vibration. We find that the p_l, and hence effective "interfacial stiffness", required for accurate fitting of the dodecane model (taking SiO_2 as the comparison) is an order of magnitude greater than that required for water. To achieve a similar change in response in ambient conditions would require a significant increase in E_{sample} of ca. 10 GPa.

We have further investigated the relation between experimental measurements and theoretical model and the influence of $E_{graphene\perp}$ and $\gamma_{graphene}$ in both ambient and dodecane environments. The Fig. 8a and Fig. 8b show the experimental ratio of UFS responses for FLG and SiO_2 (black line) that can be directly compared with simulation results (red line) in, correspondingly, ambient and dodecane environments for ultrasonic amplitude of a = 2 nm. The error (grey band) is calculated as representative standard deviation for multiple measurements at three different discrete normal forces. Our simulation show that changing E_{SiO2} had minor effect on the ratio whereas changes in the effective elasticity of the graphene

layer have much more profound effect, allowing us to fix the value of the Young's modulus of SiO_2 (table 2) while varying the Young's modulus of graphene. As seen in Fig. 8a, the best fit for ambient environment indicates the effective Young modulus of graphene $E_{graphene(amb)\perp}$ of 24.5 GPa that is 30% below the data reported in literature (table 2), whereas in dodecane environment this modulus drops to $E_{graphene(C12H26)\perp}$ = 12 GPa that is almost three times below the literature value. The best fit also suggests $\gamma_{graphene\text{-}amb}$ = 0.52 Jm^{-2} (30% higher than table 2 value) and $\gamma_{graphene\text{-}C12H26}$ = 0.03 Jm^{-2} (details on the influence of variation of $\gamma_{graphene}$ on UFS data are given in Fig. S9).

These results show that UFS effectively probes dynamic forces in the nanoscale tip-surface junctions both at separation of few monolayer distances (revealed as modification of hydration forces scaling factor p_l that add dynamic "interfacial stiffness"), as well as during full tip-surface indentation where effective Young's moduli is modified suggesting elastic "cushion" that was most profound in dodecane environment.

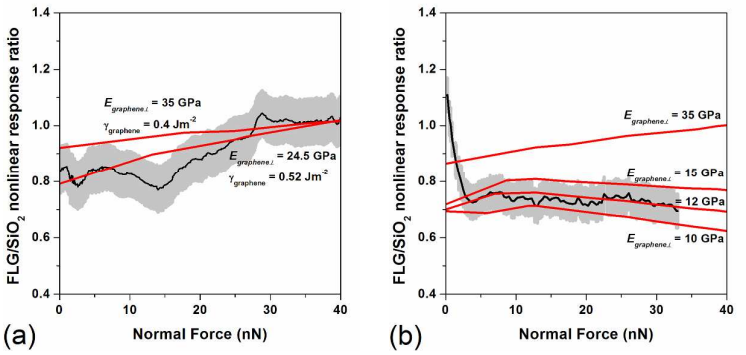

FIG 8. Comparison of FLG and SiO_2 experimental (black) and theoretical (red) nonlinear response ratios at a = 2 nm with variation of $E_{graphene\perp}$ in a) ambient conditions and b) dodecane environment. The grey region represents the associated uncertainty for the experimental responses.

Due to the hydrophobic nature of FLG[52] and the low ambient humidity (48% at 22 ^{O}C) during scanning our ambient model assumes no explicit liquid layer is present on the surface. However, this may not be true due to water meniscus formation around the hydrophilic probe.[53] A thin liquid layer on the FLG surface[24] which arise during the out of solid-solid contact portion of the ultrasonic oscillation give rise to the mismatch between literature values of $E_{graphene\perp}$ and those required to for the fitting in Fig.8. The negligible change with increasing values of E_{SiO2} suggests that rather than the mismatch resulting from stiffening of

the response due to a liquid layer on silicon it is due to cushioning on the response on FLG. The difference between the ambient and dodecane environments suggest different liquid structures arising from confined atmospheric water[54] and dodecane sub-nanometre films[55] which is consistent with previous studies[24] and not surprising given the hydrophobic nature of FLG. However, it is somewhat surprising that the stiffer dodecane film provides significantly greater cushioning effects than the water film, however this may be due to the comparison here being made between continuous dodecane layer, due to sample and probe immersion, and locally confined water, due to capillary forces at the probe apex.[56]

In summary, comparison between experiment and the interaction model with data from Tables 3 and 4, shows that we achieve excellent correlation for ambient and nonpolar environments, where the small mismatch is explained by liquid layer cushioning, but poor correlation in polar environments especially for FLG on the surface. In order to answer this question we have conducted additional experiments shedding the light on the specific dynamic nanomechanical phenomena of FLG in water.

Dynamic nanomechanical phenomena of FLG in liquids

We observe a number of inconsistencies in the nonlinear response of the FLG samples which we attribute to flake-substrate or flake-environment induced effects. For ultrasonic modulation of the lateral forces previously reported,[24] we noted almost identical behaviour for the ambient and polar environment FLG response arising from the local tip-induced water meniscus present in ambient environment. In air we observe multiple delaminations clearly visible in topographical image (Fig. 9a and Supplementary Fig. S7) as protrusions and in UFM image, Fig. 9b, as darker contrast (hence less mechanically stiff) areas revealing local suspension of the film from the substrate. On immersion of this film in either polar or non-polar liquid we find profound decrease in the number of these delaminations (Fig 9d,f). This can likely indicate a presence of a layer of liquid between the film and the substrate that facilitates reduction of friction and effective flattening of the FLG films.

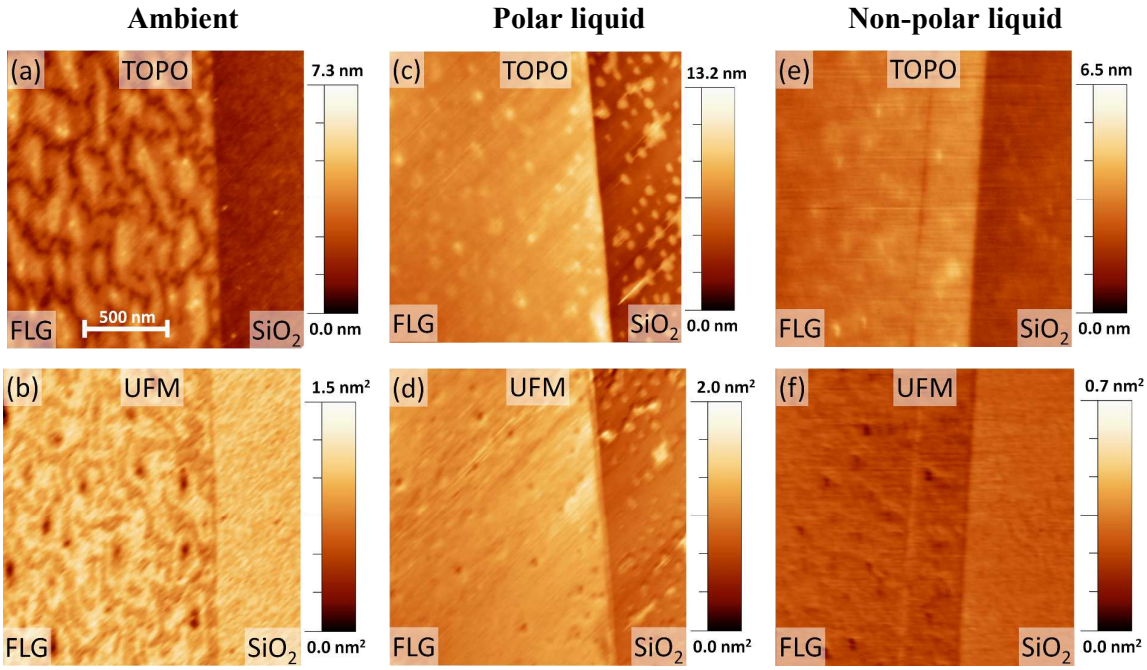

FIG 9. Contact mode topography (a,c,e) and UFM nanomechanical response (b,d,f) images of FLG and SiO2 in air(a,b), water (c,d) and dodecane (e,f) environments, all images are 1.8 x 1.8 µm. Darker contrast in UFM images correspond to less mechanically stiff areas. Note the corrugation of as-deposited graphene film in air leading to significant delaminations is clearly smoothened on immersion in liquid environment, with notably fewer low (dark spots) and high mechanical stiffness (bright spots) defects observed. Also, contamination on SiO_2 most pronounced in polar water, arising from the exfoliation process – SiO_2 measurements were performed close to but free from such features. A larger scale image of the full flake width, in ambient environment, as well as associated topographical profile are presented in in Supplementary Fig. S7.

The UFS measurements of FLG, far from the edge of the flake, compared with the simultaneously captured force-distance curves during tip retraction show a cessation of nonlinear response well before prior the tip snap out for FLG in the water immersion environment. Fig. 10a shows the nonlinear response data for FLG in water at a = 0.5nm (corresponding to the black solid line in Fig. 4a) and the simultaneously captured normal force response as function of z-position. The profound increase of the nonlinearity and its cessation (points ii to iii in Fig. 10) indicate that the solid-solid contact producing the nonlinearity becomes broken. Surprisingly, the force interaction still ranges to the distances up to 50 nm during the pull off. Similar behaviour is not observed for SiO_2 in water (see force curves in Supplementary Note 4 and Fig. S6). Interpretation of any comparable response for FLG in dodecane is inconclusive due to high degree of noise around the probe snap-out point (Supplementary Fig. S5). We believe that this two-stage snap for graphene surface indicates peeling of graphene layers under adhesion with the AFM tip.[57] Another possibility could be

that the nanobubbles of condensed gas[58, 59] are nucleated by the AFM tip on the surfaces in water due to the hydrophobic nature of the FLG surface[60] although no such behaviour was observed on well characterised hydrophobic wax surface. The length of the plateau allows us to estimate the height to which the exfoliated layer is pulled, in this case ca. 50 nm. It should be noted that, in contrast; we have observed no unusual features in the shape of the approach curves suggesting that tip-induced exfoliation is a product of the tip retraction from the substrate (Fig 10b). Exfoliation is observed during liquid immersion, but not ambient conditions despite stronger probe-sample attraction here. In ambient environment the local water is confined to the top probe-induced meniscus, however during full immersion the surrounding water is able to propagate between the stacked graphene layers, or between the graphene-SiO_2 interface [61], significantly reducing the force needed to peel, the phenomenon used to facilitate the in-liquid exfoliation of graphite[62]. These complex secondary features are not accounted for by the modelling performed above but are the likely source to the differences between experiment and theory for FLG in water.

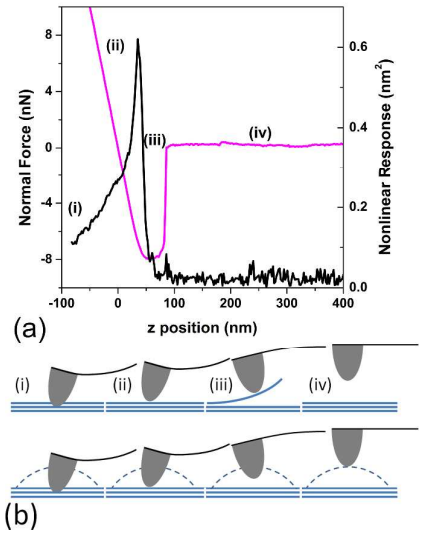

FIG 10. a) Typical UFS response (black) and normal force (pink) for FLG for the retraction branch where *a* = 0.5 nm. Different regions i-iv correspond to the proposed mechanism of graphene layer peeling (top) or nanobubble interaction (middle) shown in b)

II. Materials and Methods

1. Materials preparation and environmental parameters

Graphene samples were exfoliated from bulk Kish graphite using the well-known 'scotch tape' method prior to final exfoliation using a cross-linked polymer gel strip (Gel-Pak, USA) flakes were transfer on to freshly piranha solution (3:1 concentrated H_2SO_4 to 30% H_2O_2) cleaned and plasma treated (2% O_2, Ar) silicon substrates (300nm SiO_2 layer on Si wafer).[1] In addition, bulk Highly Ordered Pyrolytic Graphite (HOPG) was studied immediately after scotch tape exfoliation of the top few layers. All measurements were performed at room temperature (a) in an ambient laboratory atmosphere (48% humidity at 22°C), (b) with the sample and force probe immersed in ultrapure water (Millipore, Direct Q3 UV purification system), or (c) in dodecane (Alpha Aesar 99+%).

2. Ultrasonic Force Microscopy

Samples, for UFM, were mounted on a coverslip glass bonded to the piezoceramic transducer using a thin layer of salol (phenyl salicylate) resulting in near perfect coupling of longitudinal and shear ultrasonic vibrations at frequencies up to several tens of MHz.[30] Transducer mounted samples were oscillated at typically 4 MHz, well above any cantilever resonances, with a peak to peak amplitude of 0.5, 1, 2 or 4 V resulting in vertical displacements *a* of *ca*. 0.25, 0.5, 1 and 2 nm respectively as determined by laser doppler vibrometer (Polytec Inc) and is consistent with previously reported values of displacement.[29, 63] To enable detection of the 4MHz oscillation, the signal was amplitude modulated with a gated saw-tooth shaped waveform of 1.7 kHz, the cantilever deflection at this modulation frequency corresponds to the nonlinear UFM response and was subsequently detected a lock-in amplifier (Stanford Research Systems, SRS-830) as well documented in literature.[21, 63]

Simultaneously, normal force spectroscopy (approach-retract curves[64, 65]) were performed using a standard AFM contact mode cantilevers (Budget Sensors) with Scanning Electron Microscopy determined tip radii of curvature of 12.9 ± 3.7 nm. The spring constant of each cantilever was determined using the Sader method[42, 43] and were found to be with ± 15% of the manufacturers stated nominal value of 0.2 Nm^{-1}. Approach-retract curves were performed over a ramp size of 1000 nm at a vertical scan rate of 0.1 Hz in order to minimise liquid drag effects on the cantilever.[66] The AFM used was a Multimode Nanoscope III AFM (Bruker AXS) fitted with a standard liquid cell.

IV. Conclusions

In conclusion, the new method for probing nanomechanics of interfacial layers using UFS allowed us to probe solid-solid and solid-liquid-solid interactions for graphene-air and graphene-liquid environments with nanoscale resolution. Comparison of experimental data with a developed analytical model based on the DMT contact mechanics and hydration forces, indicated that while in ambient environment the stiffness of the probed layer plays a dominant role, in liquids the characteristic hydration length may be essential. By fitting the experimental UFS for graphene in water, the model shows that liquid layer effects are dominated by the first 1-3 monolayers of ordered liquid on the sample surface. At these separations the dodecane in dynamic UFS measurements at 4 MHz dynamic oscillation behaves as an additional stiff layer with a liquid layer stiffness approximately one order of magnitude greater than that of water. Furthermore, comparison of the experimental and theoretical FLG and SiO_2 nonlinear UFS response suggests that the effective Young's modulus of FLG during indentation (tip-FLG film elastic contact) is moderately reduced by 30% in ambient environment (reflecting some tip-induced water meniscus influence) whereas in full dodecane immersion it is reduced by approximately factor of 3. This very distinct change between the ambient and immersion environment is clearly linked with the effect of the liquid layer both between the tip and probably between the graphene layer and the substrate with effect more profound for the dodecane that is known to more easily produce solid-like elastic cushions while subjected to confinement. Finally, the simultaneous collection of nonlinear response and force spectroscopy allows the identification of local physical phenomena such as peeling of graphene layers providing a new tool for the elucidation of near surface physical properties of 2D materials and systems in ambient and liquid environments.

Acknowledgements:

We thank Dr Sean O'Shea (IMRE, Singapore) and Professor Paul Hansma (UCSB, USA) for fruitful discussions, OVK acknowledges support of GRENADA, FUNPROB, EPSRC EP/K023373/1 grant as well as IAA and research grants by Lancaster University.

References

1. K. S. Novoselov, A. K. Geim, S. V. Morozov, D. Jiang, Y. Zhang, S. V. Dubonos, I. V. Grigorieva and A. A. Firsov, *Science*, 2004, **306**, 666-669.

2. D. Sercombe, S. Schwarz, O. Del Pozo-Zamudio, F. Liu, B. J. Robinson, E. A. Chekhovich, Tartakovskii, II, O. Kolosov and A. I. Tartakovskii, *Sci Rep*, 2013, **3**, 3489.
3. Y. Ma, Y. Dai, M. Guo, L. Yu and B. Huang, *Phys. Chem. Chem. Phys.*, 2013, **15**, 7098-7105.
4. J. S. Bunch, A. M. van der Zande, S. S. Verbridge, I. W. Frank, D. M. Tanenbaum, J. M. Parpia, H. G. Craighead and P. L. McEuen, *Science*, 2007, **315**, 490-493.
5. C. Y. Chen, S. Rosenblatt, K. I. Bolotin, W. Kalb, P. Kim, I. Kymissis, H. L. Stormer, T. F. Heinz and J. Hone, *Nat. Nanotechnol.*, 2009, **4**, 861-867.
6. M. D. Stoller, S. J. Park, Y. W. Zhu, J. H. An and R. S. Ruoff, *Nano Lett*, 2008, **8**, 3498-3502.
7. J. J. Yoo, K. Balakrishnan, J. Huang, V. Meunier, B. G. Sumpter, A. Srivastava, M. Conway, A. L. Mohana Reddy, J. Yu, R. Vajtai and P. M. Ajayan, *Nano Lett*, 2011, **11**, 1423-1427.
8. H.-J. Choi, S.-M. Jung, J.-M. Seo, D. W. Chang, L. Dai and J.-B. Baek, *Nano Energy*, 2012, **1**, 534-551.
9. H. Park, P. R. Brown, V. Bulović and J. Kong, *Nano Lett*, 2011, **12**, 133-140.
10. X. Miao, S. Tongay, M. K. Petterson, K. Berke, A. G. Rinzler, B. R. Appleton and A. F. Hebard, *Nano Lett*, 2012, **12**, 2745-2750.
11. R. Garcia and R. Perez, *Surf Sci Rep*, 2002, **47**, 197-301.
12. R. Giridharagopal, G. E. Rayermann, G. Z. Shao, D. T. Moore, O. G. Reid, A. F. Tillack, D. J. Masiello and D. S. Ginger, *Nano Lett*, 2012, **12**, 893-898.
13. J. P. Killgore and D. C. Hurley, *Nanotechnology*, 2012, **23**.
14. U. Landman and W. D. Luedtke, *J. Vac. Sci. Technol. B*, 1991, **9**, 414-423.
15. D. Garcia-Sanchez, A. M. van der Zande, A. S. Paulo, B. Lassagne, P. L. McEuen and A. Bachtold, *Nano Lett*, 2008, **8**, 1399-1403.
16. H. Yoshizawa and J. Israelachvili, *Thin Solid Films*, 1994, **246**, 71-76.
17. S. J. Oshea, M. E. Welland and T. Rayment, *Appl. Phys. Lett.*, 1992, **61**, 2240-2242.
18. B. Bhushan, J. N. Israelachvili and U. Landman, *Nature*, 1995, **374**, 607-616.
19. K. S. Novoselov, V. I. Fal'ko, L. Colombo, P. R. Gellert, M. G. Schwab and K. Kim, *Nature*, 2012, **490**, 192-200.
20. F. M. Ohnesorge, *Surf Interface Analysis*, 1999, **27**, 379-385.
21. O. V. Kolosov and K. Yamanaka, *Japan J Appl Phys Part 2-Lett*, 1993, **32**, L1095-L1098.
22. K. K. Inagaki, OV;Briggs, GAD;Muto, S;Horisaki, Y;Wright,, *1998 IEEE Ultrasonic Symp Proc*, 1998, **VOLS 1 AND 2**, 1255-1259.
23. R. Szoszkiewicz, B. D. Huey, O. V. Kolosov, G. A. D. Briggs, G. Gremaud and A. J. Kulik, *Appl. Surf. Sci.*, 2003, **210**, 54-60.
24. B. J. Robinson, N. D. Kay and O. V. Kolosov, 2013, **29**, 7735-7742.
25. F. Dinelli, S. K. Biswas, G. A. D. Briggs and O. V. Kolosov, *Appl. Phys. Lett.*, 1997, **71**, 1177-1179.
26. M. T. Cuberes, in *Proc 17th Internat Vacuum Congr /13th Int Conf Surf Sci /Int Conf Nanosci and Techn*, eds. L. S. O. Johansson, J. N. Andersen, M. Gothelid, U. Helmersson, L. Montelius, M. Rubel, J. Setina and L. E. Wernersson, Iop Publishing Ltd, Bristol2008, vol. 100.
27. D. Kiracofe and A. Raman, *Phys. Rev. B*, 2012, **86**.
28. S. Hirsekorn, U. Rabe and W. Arnold, *Nanotechnology*, 1997, **8**, 57-66.
29. F. Dinelli, S. K. Biswas, G. A. D. Briggs and O. V. Kolosov, *Phys. Rev. B*, 2000, **61**, 13995-14006.
30. F. Dinelli, M. R. Castell, D. A. Ritchie, N. J. Mason, G. A. D. Briggs and O. V. Kolosov, *Philos. Mag. A-Phys. Condens. Matter Struct. Defect Mech. Prop.*, 2000, **80**, 2299-2323.
31. A. C. Fischer-Cripps, *Introduction to Contact Mechanics*, Springer2007.
32. B. V. Derjaguin, V. M. Muller and Y. P. Toporov, *J Colloid Interface Sci*, 1975, **53**, 314-326.
33. J. B. Pethica and W. C. Oliver, *Phys. Scr.*, 1987, **T19A**, 61-66.
34. S. Jeffery, P. M. Hoffmann, J. B. Pethica, C. Ramanujan, H. Ö. Özer and A. Oral, *Phys Rev B*, 2004, **70**, 054114.
35. Y. I. Rabinovich and R. H. Yoon, *Langmuir*, 1994, **10**, 1903-1909.
36. S. P. Koenig, N. G. Boddeti, M. L. Dunn and J. S. Bunch, *Nat. Nanotechnol.*, 2011, **6**, 543-546.

37. X.-Z. Liu, Q. Li, P. Egberts and R. W. Carpick, *Adv Mat Interfaces*, 2014, **1**, 10.1002/admi.201300053.
38. C. Greiner, J. R. Felts, Z. T. Dai, W. P. King and R. W. Carpick, *Nano Lett.*, 2010, **10**, 4640-4645.
39. B. Hajgato, S. Guryel, Y. Dauphin, J. M. Blairon, H. E. Miltner, G. Van Lier, F. De Proft and P. Geerlings, *Chem. Phys. Lett.*, 2013, **564**, 37-40.
40. J.-W. Jiang, J.-S. Wang and B. Li, *Phys Rev B*, 2009, **80**, 113405.
41. T. Toshihiro and Y. Kazushi, *Nanotechnology*, 2001, **12**, 301.
42. J. E. Sader, *J. Appl. Phys.*, 1998, **84**, 64-76.
43. J. E. Sader, J. W. M. Chon and P. Mulvaney, *Rev. Sci. Instr.*, 1999, **70**, 3967-3969.
44. S. Y. Lin, *Ultrasonics*, 2005, **43**, 365-373.
45. J. L. Bosse, P. D. Tovee, B. D. Huey and O. V. Kolosov, *J. Appl. Phys.*, 2014, **115**, 144304.
46. D. Maugis and B. Gauthiermanuel, *J. Adhes. Sci. Technol.*, 1994, **8**, 1311-1322.
47. B. Robinson, N. Kay and O. Kolosov, *Langmuir*, 2013, **29**, 7735–7742.
48. O. Kolosov, *Mater. World*, 1998, **6**, 753-754.
49. K. Porfyrakis, O. V. Kolosov and H. E. Assender, *J. Appl. Polym. Sci.*, 2001, **82**, 2790-2798.
50. Y. L. Chen, Z. H. Xu and J. Israelachvili, *Langmuir*, 1992, **8**, 2966-2975.
51. V. A. Parsegian and T. Zemb, *Curr. Opin. Coll.Interf. Sci.*, 2011, **16**, 618-624.
52. J. Rafiee, X. Mi, H. Gullapalli, A. V. Thomas, F. Yavari, Y. Shi, P. M. Ajayan and N. A. Koratkar, *Nat. Mater.*, 2012, **11**, 217-222.
53. T. Stifter, O. Marti and B. Bhushan, *Phys. Rev. B*, 2000, **62**, 13667-13673.
54. U. Raviv, P. Laurat and J. Klein, *Nature*, 2001, **413**, 51-54.
55. S. T. Cui, C. McCabe, P. T. Cummings and H. D. Cochran, *J. Chem. Phys.*, 2003, **118**, 8941-8944.
56. E. Riedo, I. Palaci, C. Boragno and H. Brune, *J Phys. Chem. B*, 2004, **108**, 5324-5328.
57. N. Sasaki, H. Okamoto, S. Masuda, K. Miura and N. Itamura, *J Nanomat.*, 2010, **2010**.
58. J. W. G. Tyrrell and P. Attard, *Langmuir*, 2002, **18**, 160-167.
59. J. W. G. Tyrrell and P. Attard, *Phys. Rev. Lett.*, 2001, **87**, 176104.
60. Y. Chih-Wen, L. Yi-Hsien and H. Ing-Shouh, *J Phys. Cond. Matt.*, 2013, **25**, 184010.
61. M. Lee, J. Choi, J.-S. Kim, I.-S. Byun, D. Lee, S. Ryu, C. Lee and B. Park, *Nano Res.*, 2012, **5**, 710-717.
62. Y. Hernandez, V. Nicolosi, M. Lotya, F. M. Blighe, Z. Y. Sun, S. De, I. T. McGovern, B. Holland, M. Byrne, Y. K. Gun'ko, J. J. Boland, P. Niraj, G. Duesberg, S. Krishnamurthy, R. Goodhue, J. Hutchison, V. Scardaci, A. C. Ferrari and J. N. Coleman, *Nat. Nanotechnol.*, 2008, **3**, 563-568.
63. I. Grishin, B. D. Huey and O. V. Kolosov, *ACS Appl. Mater. Interfaces*, 2013, **5**, 11441-11445.
64. N. A. Burnham, R. J. Colton and H. M. Pollock, *Nanotechnology*, 1993, **4**, 64.
65. B. Capella, P. Baschieri, C. Frediani, P. Miccoli and C. Ascoli, *IEEE Eng. Med. Biol. Mag.*, 1997, **16**, 58-65.
66. E. F. de Souza, R. A. Douglas and O. Teschke, *Langmuir*, 1997, **13**, 6012-6017.

Table of contents entry

The study of interfacial forces in graphene-air and graphene-liquid environments with nanoscale resolution by experimental and theoretical development of novel ultrasonic force spectroscopy (UFS).